Diagnostic tools for evaluating quasi-horizontal transport in global-scale chemistry models

Huikyo Lee,[1,2] Daeok Youn,[3] Kenneth O. Patten,[1] Seth C. Olsen,[1] and Donald J. Wuebbles[1]

Received 19 February 2012; revised 23 August 2012; accepted 23 August 2012; published 2 October 2012.

[1] The upper troposphere and lower stratosphere (UTLS) plays an important role in climate and atmospheric chemistry. Despite its importance on the point of causing deep intrusions of tropics originated air into the midlatitudes, the quasi-horizontal transport process in the UTLS, represented by global chemistry-transport models (CTMs) or chemistry-climate models (CCMs), cannot easily be diagnosed with conventional analyses on isobaric surfaces. We use improved diagnostic tools to better evaluate CTMs and CCMs relative to satellite observations in the region of UTLS. Using the Hellinger distance, vertical profiles of probability density functions (PDFs) of chemical tracers simulated by the Model for OZone And Related chemical Tracers 3.1 (MOZART-3.1) are quantitatively compared with satellite data from the Microwave Limb Sounder (MLS) instrument in the tropopause relative altitude coordinate to characterize features of tracer distributions near the tropopause. Overall, the comparison of PDFs between MLS and MOZART-3.1 did not satisfy the same population assumption. Conditional PDFs are used to understand the meteorological differences between global climate models and the real atmosphere and the conditional PDFs between MOZART-3.1 and MLS showed better agreement compared to the original PDFs. The low static stability during high tropopause heights at midlatitudes suggests that the variation of tropopause height is related to transport processes from the tropics to midlatitudes. MOZART-3.1 with the GEOS4 GCM winds reproduces episodes of the tropical air intrusions. However, our diagnostic analyses show that the GEOS4 GCM did not properly reproduce the high tropopause cases at midlatitudes especially in spring.

Citation: Lee, H., D. Youn, K. O. Patten, S. C. Olsen, and D. J. Wuebbles (2012), Diagnostic tools for evaluating quasi-horizontal transport in global-scale chemistry models, *J. Geophys. Res.*, *117*, D19302, doi:10.1029/2012JD017644.

1. Introduction

[2] Spatial distributions and temporal variations of radiatively active chemical species near the tropopause play a key role in the Earth's climate system. A number of studies have shown that surface temperature is strongly affected by the radiative influence of near-tropopause ozone (O_3) [e.g., *Lacis et al.*, 1990; *Forster and Tourpali*, 2001] and water vapor (H_2O) [e.g., *Forster and Shine*, 2002; *Solomon et al.*, 2010]. The representation of chemical and transport processes affecting O_3 and H_2O in the upper troposphere and lower stratosphere (UTLS) is thus important in assessing the potential impact of human-produced emissions, including aviation emissions.

[1]Department of Atmospheric Sciences, University of Illinois at Urbana-Champaign, Urbana, Illinois, USA.

[2]Now at Jet Propulsion Laboratory, California Institute of Technology, Pasadena, California, USA.

[3]Department of Earth Science Education, Chungbuk National University, Cheongju, South Korea.

Corresponding author: D. Youn, Department of Earth Science Education, Chungbuk National University, Cheongju, Chungbuk 361-763, South Korea. (dyoun@chungbuk.ac.kr)

0148-0227/12/2012JD017644

[3] Stratosphere-troposphere exchange (STE) is an important factor in determining the distribution of ozone and other trace constituents in the UTLS [e.g., *Chen*, 1995; *Cristofanelli et al.*, 2003]. Therefore, model evaluation of the potential effects of aviation emissions on ozone and climate is critically dependent on the representation of STE in models. Tracer exchange between the troposphere and the stratosphere occurs through three major pathways [*Holton et al.*, 1995; *Dessler et al.*, 1995; *Strahan et al.*, 2007]. The first is the Brewer-Dobson circulation which is characterized by tropospheric air rising through the tropical tropopause and stratospheric air descending at mid and high-latitude. The second is tropopause folding caused by secondary circulation across fronts [*Holton et al.*, 1995]. Finally, the third is quasi-isentropic horizontal transport between the 'lowermost stratosphere' at midlatitudes [*Holton et al.*, 1995] and the 'tropically controlled transition region' in the tropics [*Rosenlof et al.*, 1997]. The extratropical route for the quasi-isentropic horizontal transport provides a two-way transport for chemically and radiatively important trace constituents between the tropical upper troposphere and the midlatitudes lower stratosphere. Although this STE process is more frequent in winter due to stronger wave activities [*Gettelman et al.*, 2011], deeper intrusions of the air from the tropics into the midlatitudes

occur in summer [*Pan et al.*, 2009]. Large synoptic systems such as monsoon anticyclones can enhance the exchange of air between the tropical troposphere and the midlatitudes stratosphere [*Chen*, 1995; *Gettelman et al.*, 2004] and a recent study by *Manney et al.* [2011] highlighted the role of jet streams in this STE process.

[4] Three-dimensional global chemistry transport models (CTMs) and chemistry climate models (CCMs) have been used to study atmospheric chemistry processes in the UTLS for some time and these modeling capabilities have been substantially improved in recent years. The Chemistry-Climate Model Validation (CCMVal) 2 project [*Eyring et al.*, 2010] suggested useful tools applicable to the UTLS [*Gettelman et al.*, 2010; *Hegglin et al.*, 2010]. The diagnostic tools in CCMVal 2 can be used not only to evaluate models but also to provide better understanding of the processes affecting the UTLS.

[5] Satellite data sets are often used for the evaluation of model chemistry and dynamics in the UTLS region. Satellite data provide extremely useful information for chemistry model evaluation in the UTLS on a global scale [e.g., *Pan et al.*, 2007]. *Pan et al.* [2009] has shown that high vertical resolution data from High Resolution Dynamics Limb Sounder (HIRDLS) can be utilized to demonstrate the dynamics of STE processes. *Hegglin et al.* [2009] used the Atmospheric Chemistry Experiment – Fourier Transform Spectrometer (ACE-FTS) data with vertical resolution of 1–3 km to scrutinize the structure of key chemical species in the UTLS. *Kim and Son* [2012] used high resolution temperature profiles from GPS satellites to investigate the climatological structure of the tropical tropopause. The Microwave Limb Sounder (MLS) onboard the NASA Earth Observing System (EOS) Aura platform provides global information on O_3, carbon monoxide (CO) and H_2O daily and these measurements have been used in studies on the UTLS. For example, upper tropospheric CO was compared with the GEOS-CHEM CTM in *Li et al.* [2005]. MLS O_3 in the upper troposphere was used to estimate tropospheric column ozone (TCO) and the TCO was compared with the NASA Global Modeling Initiative (GMI) Combo CTM results, showing good agreement in terms of zonal variation and seasonal cycle [*Ziemke et al.*, 2006]. *Strahan et al.* [2007] analyzed various transport diagnostics for the lowermost stratosphere to evaluate CTMs, including the use of MLS data for concentrations of O_3 and N_2O. *Manney et al.* [2011] found good agreement between MLS data and ACE-FTS in the UTLS. Using seven years of MLS data, *Santee et al.* [2011] has comprehensively shown the seasonal and interannual variations of key tracers along with a broad overview of MLS trace gas observations in the lowermost stratosphere. However, even the latest version of MLS data has coarse vertical resolution compared to the vertical scale of variability in the UTLS. Therefore, any diagnostic tools using MLS data need to overcome the limitation of its low vertical resolution. For example, previous studies [*Manney et al.*, 2007; *Santee et al.*, 2011] made extensive use of meteorological data from assimilation and reanalysis data, collocated with satellite observations to calculate potential temperature, potential vorticity, and equivalent latitude and to estimate tropopause height.

[6] Another issue of concern in the comparison of model simulation outputs with satellite observations is the difference in background meteorology between the satellite observations and model simulations. All CCMs generating their own meteorological fields have different tracer distributions with observations partially due to this difference. CTMs can somewhat avoid this issue by using assimilated meteorological fields and using assimilation data is common and best to run CTMs for most of studies. Although the diagnostic tools used in this study can be applied to CTMs driven with assimilated data, the diagnostic tools used in this study are aimed at application to CTMs driven by GCM meteorology and CCMs. So the tools were designed to consider the differences of meteorological field between the modeled and observed atmosphere.

[7] In this study, through the adaptation and extension of previously developed diagnostic tools, we introduce a practical approach for evaluating the performance of global CTMs and CCMs representing quasi-isentropic transport processes in the UTLS region. Our improved approach utilizes a set of diagnostic tools designed to take advantage of the merits of MLS data while overcoming some difficulties in applying it in the UTLS. In this study these tools are applied to the equatorial region (5°S–5°N) and the midlatitudes region (40°N–50°N) in the Northern Hemisphere (NH) during the summer (JJA) when the horizontal mixing near the tropopause is enhanced by monsoon anticyclone activity [*Strahan et al.*, 2007]. Because a single isobaric level cannot show isentropic motions, we examine multiple isobaric levels simultaneously. Our tools can be applied to the comparison and evaluation of any global-scale CTMs or CCMs relative to satellite data. In this study, we chose one set of representative CTM and satellite data and analyzed them as an example to demonstrate the usefulness of our approach. The evaluation of a CTM with reasonable chemical reactions and dynamical cores for tracer transport is in fact an evaluation of input meteorological fields. The remainder of this paper is structured as follows. The analysis techniques and the model and observational data used for our improved diagnostic tools are described and discussed in section 2 and section 3 respectively. Comparisons between the model simulations and MLS observations are presented in section 4 and finally the key findings are summarized in section 5.

2. Analysis Technique

[8] To facilitate model evaluation in the UTLS and account for the sharp vertical gradients of tracers across the tropopause, we adopt the thermal-tropopause relative height (hereafter TPRH) vertical coordinate system and use probability density functions (PDFs) in the TPRH coordinate. Both model outputs and observational data in the TPRH coordinate, rather than in the conventional isobaric vertical coordinate, better represent the vertical structure of tracer distributions near the tropopause and are thus useful to evaluate the performance of models in the UTLS [*Hoor et al.*, 2004; *Pan et al.*, 2007; *Hegglin et al.*, 2009]. Between the two commonly used definitions of tropopause, the thermal and the dynamical tropopause, the thermal tropopause is used following the definition of the *World Meteorological Organization* (*WMO*) [1957] as in *Son et al.* [2009]. However, it is difficult to accurately determine the tropopause from temperature data from model outputs with low vertical resolution in the tropopause region. We adopt an accurate and robust method to determine the tropopause

height from gridded model data with low vertical resolution as suggested by *Reichler et al.* [2003]. The method has the advantage that it can be applied globally based on the local vertical profile of atmospheric temperature in a consistent manner. The method is briefly described here.

[9] Starting from the temperature (T) on pressure levels p, the lapse rate is calculated as:

$$\Gamma(p) = \frac{\partial T}{\partial p^{\kappa}} \frac{p^{\kappa}}{T} \left(\frac{\kappa g}{R}\right) \tag{1}$$

where $\kappa = R/c_p$, R is the gas constant for dry air, c_p the specific heat capacity of air at constant pressure, and g is the gravitational acceleration. Using linear interpolation between any two pressure levels, the first tropopause (i.e., the conventional tropopause) can be found as the lowest level, where the lapse rate of below 2 K km^{-1} appears and the average lapse rate of all higher levels within 2 km does not exceed 2 K km^{-1}. If the latter does not hold, one proceeds to the next higher level until the criteria are satisfied. In some model or data columns, the lapse rate for a level more than 2 km above this first tropopause may exceed 2 K km^{-1}. If so, a second tropopause could be defined at the next level having a lapse rate less than 2 K km^{-1} using the same criteria as for the first tropopause and the average lapse rate over all levels within 2 km above does not exceed 2 K km^{-1}. In practice, the tropopause for model data used to run CTMs is likely to be well defined using this method. Lower and upper limits of the tropopause pressure are chosen to be 450 hPa and 75 hPa respectively.

[10] After determining the thermal tropopause height, the geopotential distances between the pressure level of the tropopause and levels above/below the tropopause were calculated to find the TPRH. Considering the MOZART-3.1 vertical resolution of about 1.1 km, the model output were vertically gridded with the resolution of 1.1 km from the tropopause (TPRH = 0) after being collected and averaged within the grid box of 1.1 km height.

[11] PDFs have been used in many previous studies for evaluating models using observations. *Sparling* [2000] has shown examples of the application of PDFs to investigate transport processes since each process is represented as a different mode in the PDFs. To compare the variability of aircraft-observed and model-simulated O_3 and CO concentrations, *Emmons et al.* [2000] made use of PDFs of the data in the troposphere. In analyzing aircraft-measured O_3 in the UTLS, *Ray et al.* [2004] used PDFs to consider outliers while showing predominant features of data. *Strahan and Polansky* [2006] analyzed methane (CH_4) PDFs to compare latitudinal distributions of CH_4 relative to simulations using the GMI CTM and investigated transport characteristics of the model. *Strahan et al.* [2007] compared GMI simulations with MLS data sets for nitrous oxide using PDFs for each season as transport diagnostics. *Hegglin et al.* [2010] identified depth of the extratropical tropopause transition layer using PDFs of H_2O. PDFs, therefore, can be more useful to compare broad characteristics of tracer distributions than simply comparing averaged values and standard deviations, especially when the tracer distributions are skewed relative to bell-shaped distributions. For quantitative comparisons between PDFs from different sources, the Hellinger distance [*Rieder*, 2005; *Tilmes et al.*, 2011] was calculated. For two probability density functions, f(x) and g(x) with the same bin size, the Hellinger distance, H, is defined as:

$$H = \left[\frac{1}{2}\int \left(\sqrt{f(x)} - \sqrt{g(x)}\right)^2 dx\right]^{0.5} \tag{2}$$

The values of H range from zero to 1 and smaller H values indicate more similarity between two PDFs as shown in Figure 1. However, it should be noted that H is a relative metric. Values of H depend on the size of data intervals for discrete PDFs so there is no pre-defined benchmark H value to represent good agreement at a high confidence level. Therefore, we empirically determine reference H values indicating good agreement by conducting Monte Carlo simulations. For example, the PDFs with red and blue lines in Figure 1 are a reference and a target PDF respectively. Both reference and target data consist of 3,000 randomly generated values.

[12] First, we subsampled 1,500 data out of 3,000 reference data twice allowing replacement and calculated H between the two subsamples. H is close to zero because they are from the same original data. This process was repeated 1,000 times and the resulting distribution of H values between the subsamples are shown in Figure 1d. The average of H over these subsamples is 0.076. We interpreted this value as averaged Hellinger distance variation related to internal variability of the reference data. In other words, on average, 0.076 of departures from H = 0 can occur even for PDFs from the same reference population in this example. We define this average H as the threshold. By applying the Kolmogorov-Smirnov test which is a popular tool to test the same population assumption between two PDFs [*Corder and Foreman*, 2009], we checked that H values smaller than the threshold correspond to small K and large p-value as denoted in Figure 1b. Therefore, when an H between two PDFs is less than the threshold value defined using reference data, it is possible to say that the PDFs are drawn from the same underlying distribution.

[13] We carried out another Monte Carlo simulation from a set of samples created by mixing up the reference and target data, using the threshold H to represent a good agreement between two PDFs. Each mixed sample includes 3,000 data points. The x axis of Figure 1e shows the ratio of how much data in the mixed sample comes from the target PDF. As we increased the ratio from 0 to 100% in 1% increments, we resampled one hundred times and Hellinger distance was calculated for each resampling and plotted in Figure 1e. Not surprisingly, the Hellinger distance increases as the mixed sample has less data from the reference and there is an almost linear relationship. When the ratio equals 100%, the data is the same as the target data so Hellinger distance is 0.187 as originally calculated. Here, we define a new metric S as the ratio of the threshold Hellinger distance to the original Hellinger distance. In this case, S = 0.076/0.187 = 41% meaning that up to 41%, taking data from the target data and mixing it up with the reference data does not make significant changes in H. Comparing H values among different cases is useful only when their reference PDFs are same. For

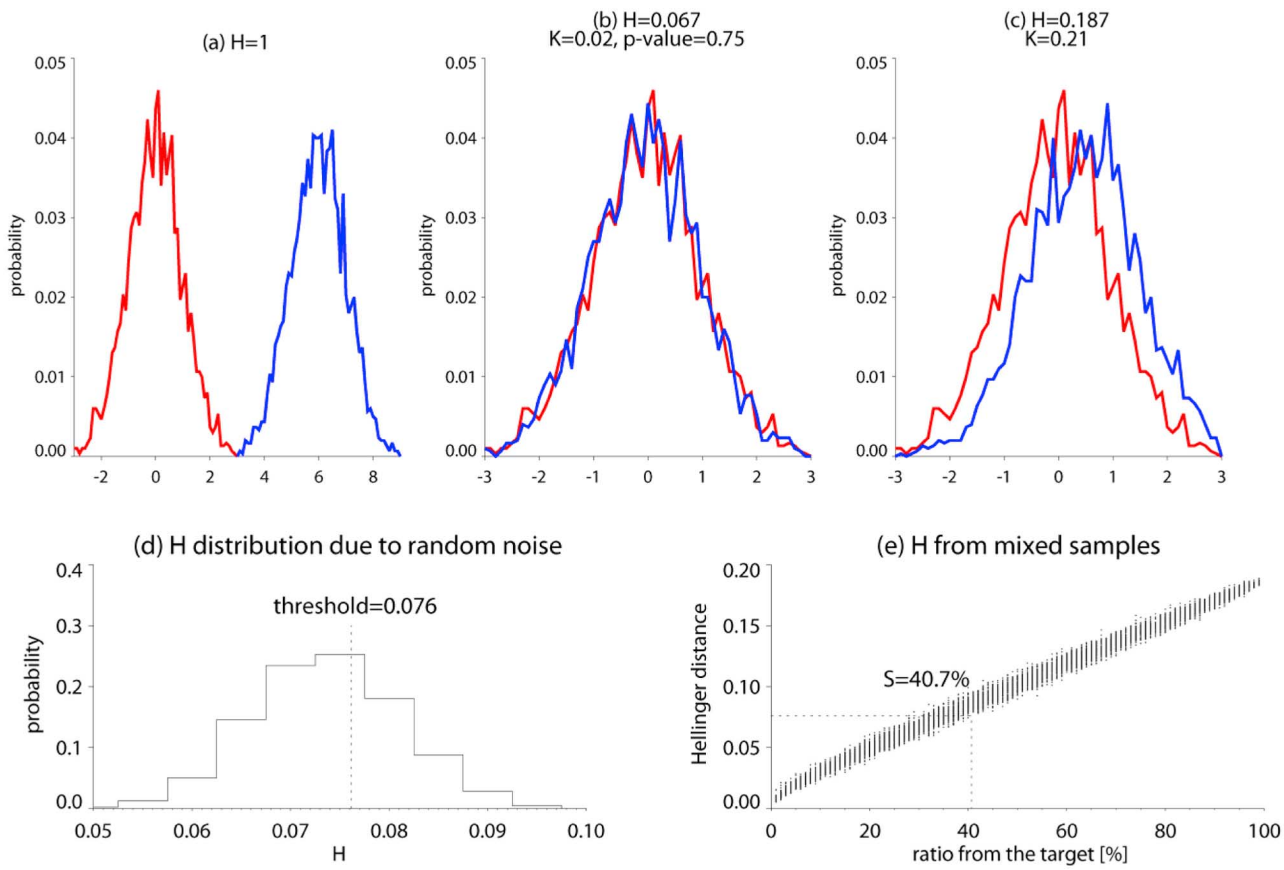

Figure 1. (a, b, and c) Hellinger distances (H), K metric from Kolmogorov-Smirnov test and corresponding p-value between a reference (red) and target (blue) probability distribution functions (PDFs). Probability density functions were randomly generated. (d) The distribution of H between 1,000 pairs of two half-sized subsamples from the reference data. (e) H between two samples which are mixture of the reference and target data. The ratio of target data in the mixed sample increases from 0 to 100% with a 1% interval.

example, with four PDFs A, B, C and D, we can compare similarity of B and C to A by comparing H from A and B with H from A and C. However, H between A and B is not comparable with H between C and D. In this case, S can be more universally applicable because it considers interval variability of reference data itself. Contrary to H, larger S values mean better agreement between two PDFs. However, S is still a relative metric and we should not assign too much meaning to this value itself. Using S to compare PDFs is a quantitative improvement compared with the previous study of discussing qualitative similarities in a pattern of PDFs [e.g., *Strahan et al.*, 2007, Figure 4].

[14] Tracer-tracer correlations in the UTLS have previously been used to effectively explore STE processes, especially at midlatitudes [*Fischer et al.*, 2000; *Zahn et al.*, 2000; *Zahn and Brenninkmeijer*, 2003; *Hoor et al.*, 2002, 2004; *Pan et al.*, 2004, 2007; *Sankey and Shepherd*, 2003; *Hegglin and Shepherd*, 2007]. As a different approach from previous studies, here we use two dimensional correlation maps instead of scatterplots to better analyze the correlation between the tracer transition at each TPRH level and regional characteristics near the UTLS. Correlation maps between tropopause heights and O_3 have been analyzed and are discussed in sections 4.2.

3. Model and Data Description

3.1. Model

[15] For the initial application of the diagnostic techniques described in the previous section, we chose the National Center for Atmospheric Research (NCAR) Model for Ozone And Related chemical Tracers (MOZART) version 3.1 as a representative CTM for the UTLS analyses. The MOZART-3.1 is a global CTM that represents relevant chemistry and physical processes affecting atmospheric composition in the troposphere and stratosphere [*Kinnison et al.*, 2007; *Pan et al.*, 2007] and has been used for many studies of atmospheric processes [*Wuebbles and Patten*, 2009; *Youn et al.*, 2009, 2010; *Tilmes et al.*, 2010] and participated in many model intercomparisons so its performance has been well characterized [e.g., *Liu et al.*, 2009]. The reactive chemical system in MOZART-3.1 includes 106 species, and 71 photolytic and 238 chemical reactions. The atmospheric constituents whose tropospheric and stratospheric distributions are simulated in the model include O_3, H_2O, hydrogen oxide radicals, nitrogen oxides, halogens, hydrocarbons, and various aerosols. For transport of chemical species and hydrological cycle, MOZART-3.1 uses meteorological information from a GCM or from a data assimilation system (DAS).

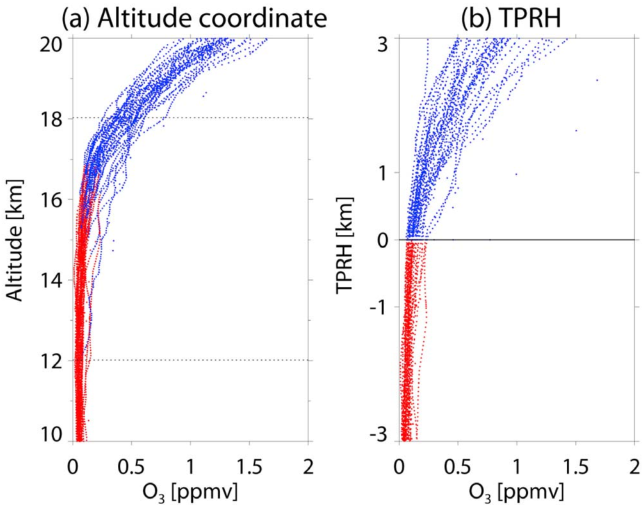

Figure 2. O_3 profiles from WOUDC ozone sonde measurements near Tsukuba in Japan (36°N, 140°E) for every September between 1994 and 2005. Profiles are shown in (a) altitude coordinate and in (b) TPRH. Red and blue dots indicate values in the troposphere and stratosphere respectively. Two dotted lines in Figure 2a represent range of tropopause heights.

Although CCMs are more generally used projecting future changes in the environment, CTMs driven by reliable GCM winds and temperatures can be used for the evaluation and improvement of our current understanding of the UTLS while being more computationally efficient than CCMs.

[16] For this study, the MOZART-3.1 simulation was driven by meteorological fields from the NASA Global Modeling and Assimilation Office (GMAO) Goddard Earth Observing System 4 AGCM (GEOS4 GCM) forced by observed sea surface temperature for 1998. The GEOS4 GCM has approximately a 2.5° (longitude) × 2.0° (latitude) horizontal grid and a hybrid-sigma coordinate system including 42 vertical levels from the surface to an upper boundary at 0.015 hPa. Assuming the constant scale height of 7 km, the vertical resolution of the meteorological fields and output of MOZART-3.1 is about 1.1 km between the top of planetary boundary layer and lower stratosphere (altitude of 3–20 km). The same meteorological data were used in earlier studies with the GMI model [*Strahan et al.*, 2007; *Considine et al.*, 2008].

3.2. Observational Data Sets

[17] The MLS instrument on the NASA EOS Aura satellite is a passive instrument consisting of several radiometers. MLS science data operations began on 13 August, 2004 [*Waters et al.*, 2006]. As MLS field-of-view (FOV) is scanned vertically through the atmospheric limb, it makes vertically resolved measurements of trace gases; the vertical coverage varies for each constituent. For O_3, CO, H_2O, and temperature used in this study, retrieved values on or above 261 hPa have been shown to be reliable for the latest version of Aura MLS Level 2, Version 3.3 (v3.3) [*Livesey et al.*, 2011]. A daily total of about 3400 profiles exist with along-track horizontal resolution of 1.5 degrees. The latitude coverage is near global from 82°S–82°N.

[18] Aura MLS v3.3 has many improvements over Version 2.2 such as higher vertical resolution between 316 hPa and 1 hPa for O_3 and H_2O [*Livesey et al.*, 2011]. Previous versions of MLS data had coarse vertical resolution (3–4 km) for O_3 in the UTLS. MLS v3.3 data released in early 2011 have a vertical resolution of less than 3 km in the UTLS region for O_3 and H_2O, while the vertical resolution for CO (3–4 km) is the same as in version v2.2. The vertical resolution of O_3 was improved while the horizontal resolution became poorer than the previous version. In the UTLS, the reported precision of CO and O_3 is about 15 ppbv and 20–40 ppbv, respectively. For water vapor, single-profile precisions are 40, 20, and 15% at 215, 147, and 100 hPa, respectively.

[19] Six years of MLS v3.3 data between January 2005 and December 2010 were used in this study for three chemical species (O_3, CO, and H_2O), temperature, and tropopause heights. We followed all screening recommendations in *Livesey et al.* [2011]. Due to the coarse vertical resolution of MLS temperature, the tropopause height included in MLS was inferred from assimilated temperature fields from NASA GMAO GEOS-5 [*Manney et al.*, 2007] following the World Meteorological Organization (WMO) definition [*WMO*, 1957]. Approximate altitudes were calculated with 7 km of scale height as used for MOZART-3.1. Using the tropopause height and approximate altitude, the MLS data at isobaric levels were also vertically rearranged in the TPRH with the same vertical resolution of 1.1 km as MOZART-3.1.

[20] O_3 and temperature data, provided by the World Ozone and Ultraviolet Radiation Data Center (WOUDC) ozonesonde database, were also used here for the period January 1994 to December 2005. This data has a much longer observational record and finer vertical resolution (less than 100 m) than MLS (about 2.5–3 km). Therefore, O_3 profiles of 12 years from WOUDC stations in the tropical Indian Ocean (in Figure 5) and in one Japanese station (in Figure 2) were used to validate both MLS and MOZART-3.1.

4. Results

4.1. Comparison of Probability Density Functions

[21] We compared the differences between the vertical structures of O_3 near the tropopause in a geometric altitude and the TPRH coordinates. Figure 2 shows O_3 profiles from WOUDC ozone sonde measurements near Tsukuba in Japan for every September between 1994 and 2005. Over 12 years of observation period, the tropopause height in September varies between 12 and 18 km. As shown in Figure 2b, ozone profiles in the TPRH coordinate are more scattered at heights in the lower stratosphere (blue dots) than those in a geometric altitude coordinate at comparable heights. This is a different result from previous studies.

[22] *Pan et al.* [2004, 2007] noted that, in using the TPRH coordinate, the vertical profiles of O_3 near the tropopause are much more compact and CO shows steeper vertical gradient than those using altitude coordinates. *Hegglin et al.* [2008] also showed relatively more compact vertical profiles of O_3 near the tropopause. However, as shown in Figure 2, rearrangement of tracer vertical profiles in the TPRH coordinate system does not always make vertical profiles compact, and the range of TPRH where a large scatter appears is different for different tracers. For example, vertical profiles of CO in a geometric altitude coordinate are more compact

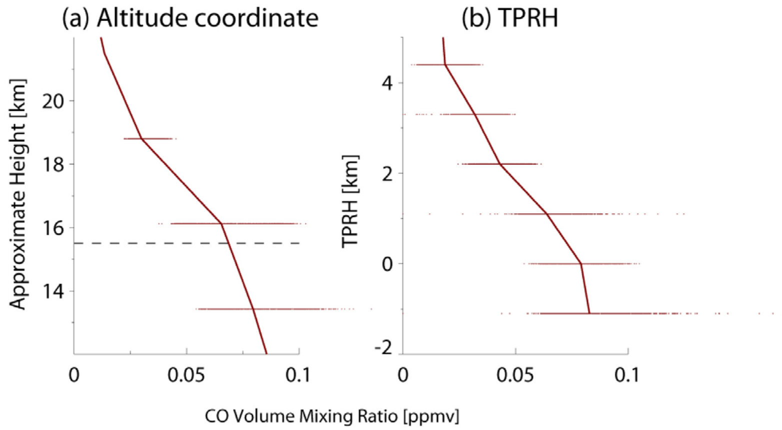

Figure 3. Zonally and monthly averaged vertical profiles of MLS CO from 25°N in July. Scattered points are observed values from measuring locations within ±5 degrees from the given center latitude. (a) isobaric vertical coordinate and (b) TPRH. The dotted line in Figure 3a shows mean tropopause levels.

below the tropopause than those in the TPRH coordinate. The larger variability of tracer profiles at a station seen in the TPRH coordinate may indicate important features which are hidden or unclear when viewing the data in conventional altitude coordinates. In the following section, we will show that the scattered distributions of tracer mixing ratios in the TPRH coordinate are related to the quasi-horizontal transport between tropics and midlatitudes.

[23] When observed data or model simulated output are sorted for a certain period and rearranged vertically in the TPRH coordinate, a representative vertical profile shows a better resolved vertical structure in the UTLS. Figure 3 shows the advantage of using TPRH coordinates. The left panel shows that MLS data has retrieved values at most two or three isobaric levels in the UTLS. However, when original MLS data from a range of latitudes in July were collected and rearranged in TPRH vertical coordinate with a resolution of 1.1 km as in Figure 3b, the original data at the same isobaric level were subdivided into those at more levels according to the values of tropopause height (TPRH = 0) in the TPRH system. For example, data on the isobaric surface of 261 hPa can be 2 km below or 1 km above the tropopause (TPRH) depending on the local tropopause height. Accordingly, we can have one population of profiles for which a pressure level in the UTLS region is above the tropopause and the other population for which the same level is below the tropopause.

[24] As shown in Figure 3, for the investigation of scientific features in the UTLS region where tracer profile data have coarse vertical resolution with steep vertical changes, the adoption of the TPRH coordinate is shown to be advantageous in revealing tracer distributions. However, it must be noted that using TPRH does not actually give finer vertical resolution but representing the profiles in the TPRH coordinate can reveal vertical structure across the tropopause, not seen when represented in geometric coordinates.

[25] Comparisons of tracer PDFs from the MOZART-3.1 simulation and MLS observations are made to evaluate the model's capability to reproduce observed tracer distributions with meteorological fields from GEOS4 GCM. However, to fully exploit usefulness of the PDF comparisons, it is important to check the statistical robustness of the PDFs [*Sparling*, 2000].

[26] Figure 4 shows two PDFs of O_3 mixing ratio profiles collected at a latitude range of 40°N–50°N and TPRH levels of −1.1–6.6 km for the NH summer (June–August, JJA). The PDFs in Figure 4 are calculated using all retrieved MLS v3.3 data between 2005 and 2010 (left plot) and randomly sub-sampled 23027 profiles out of the total 112872 profiles over five years (right plot). An orange color denotes higher probability and a blue color denotes lower probability. Almost perfect agreement between the maps of O_3 PDFs in Figure 4 indicates that the shape of the PDF is not affected by randomly adding or subtracting a fraction of the observations. This is also true in other seasons (not shown). Hellinger distances between the two PDFs are almost zero at all levels displayed in Figure 4. The advantage of using PDFs instead of conventional vertical profiles is that important characteristics such as multiple peaks can be clearly distinguished, for example, as seen with O_3 in Figure 4 at around the 5 km level. Because the shape of the PDFs has a seasonal cycle at midlatitudes, we compare PDFs from MLS and MOZART-3.1 for all four seasons but focus mostly on the NH summer.

[27] In order to characterize the effects of the quasi-horizontal STE processes, we analyzed two regions, the tropics (5°S–5°N) and the midlatitudes (40°N–50°N). Based on climatological tracer distributions, these two regions represent the lower and higher latitude zones divided by the subtropical transition zone. Figure 5 shows vertical distribution of tropical O_3 PDFs from MLS, MOZART-3.1 and WOUDC in JJA. The lines in Figure 5 connect the most probable values of PDFs at each TPRH level. Tropical O_3 from both the model and observations commonly show a sharp increase and large variability above the 4.4 km TPRH and there is a layer with less strong vertical gradient between 2.2 and 4.4 km TPRH. Overall, MOZART-3.1 shows poor agreement when comparing the distribution of O_3 with WOUDC. The S values smaller than 100% indicate that the PDFs from both MLS and MOZART-3.1 cannot satisfy the same population assumption when compared with WOUDC PDFs. By comparing S-values, we can compare similarity between PDFs at

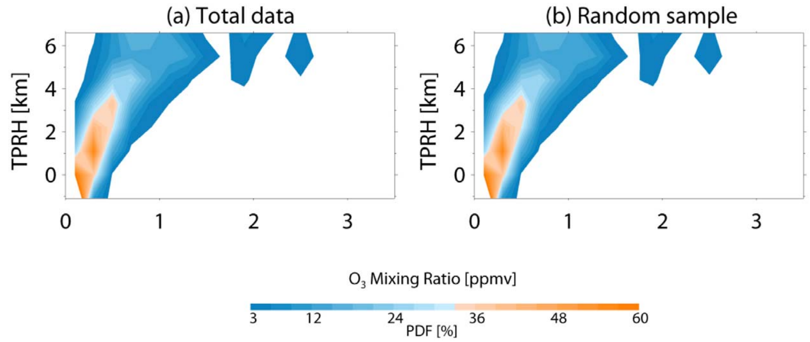

Figure 4. Vertical distribution of O_3 PDFs at NH midlatitudes (40°N–50°N) from MLS in JJA (June, July and August) when the TPRH is used as a vertical coordinate. (a) PDF using all retrieved level 2 data between 2005 and 2010 and (b) PDF using randomly sub-sampled 23027 profiles out of the total 112872 profiles.

different TPRH levels. Both MLS and MOZART-3.1 show the best agreement at the tropopause level (TPRH = 0) followed by TPRH = 2.2 km in MLS and TPRH = 5.5 km. It is interesting that the H values of MLS at TPRH = 5.5 km (H = 0.4) and at 3.3 km (H = 0.2) have almost the same S values of about 7.5%. This is caused by larger variability of the WOUDC O_3 PDF at 5.5 km.

[28] In Figure 6, H_2O PDFs between MOZART-3.1 and MLS show relatively good agreement at lower TPRH levels. At and above the 4.4 km in the TPRH, S is smaller than 1%. Unlike the O_3 PDFs, the H_2O PDFs in the tropics vary with season. This seasonal variation is present both in MOZART-3.1 and MLS H_2O PDFs in the lower stratosphere. This is related to the seasonal variation of cold point temperature at the tropical tropopause [e.g., *Mote et al.*, 1995] and it is shown reasonably in MOZART-3.1 and MLS as described below.

[29] Figure 7 shows that the tropical tropopause temperature in the NH winter (DJF) is lower than that in summertime (JJA) both in the model and observations. As a result, more water vapor freezes out of the air before it enters the stratosphere through the Brewer Dobson circulation in the NH winter and spring than in summer and fall. Lower stratospheric H_2O in MOZART-3.1 shows a clear seasonal variation according to a distinctive cold point temperature distribution of GEOS4 GCM temperature fields. Cold point temperatures observed by WOUDC sondes also display this variability. Despite the overall disagreement, the cold point temperature shows better agreements between MLS and MOZART-3.1 in DJF than JJA. In Figure 6, the relatively large difference in JJA is displayed with larger Hellinger distances and smaller S below the 3.3 km in TPRH. This implies that disagreement in the cold point temperature in Figure 7 could cause significant H_2O differences in the lower

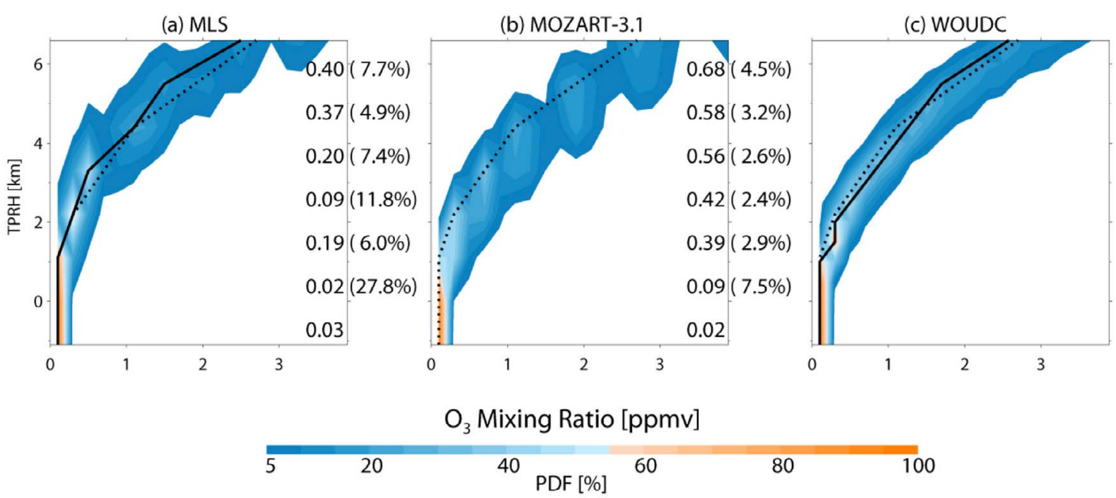

Figure 5. Vertical distribution of O_3 PDFs in the tropics (5°S–5°N) for JJA from (a) MLS, (b) MOZART-3.1 results and (c) WOUDC ozone sondes. WOUDC sonde data is only for the tropical Indian Ocean (10°S–10°N and 30°E–120°E). The solid lines connect the most probable values of MLS and WOUDC O_3 at each TPRH range while the dotted lines in Figures 5a, 5b and 5c commonly show the most probable values in MOZART. Numbers shown in the plots are Hellinger distance and corresponding S values from the WOUDC PDFs at relative altitude levels.

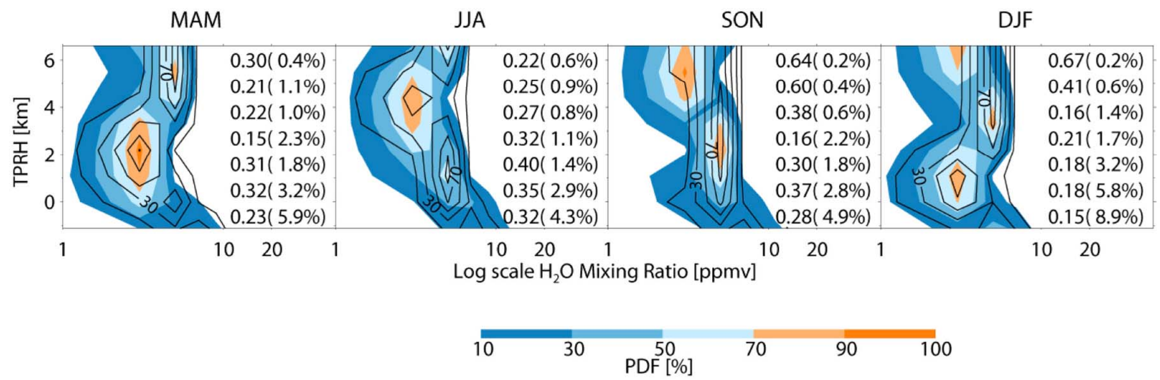

Figure 6. Vertical distributions of H_2O PDFs in the tropics (5°S–5°N). PDFs were made for (left to right) March to May, June to August, September to November and December to February. The shades and contour lines are from MLS and MOZART-3.1 respectively. Numbers shown in the plots are Hellinger distance and corresponding S values of PDFs between MLS and MOZART-3.1.

stratosphere and the differences become greater at higher altitudes.

[30] For the midlatitudes region, O_3 PDFs are presented in Figure 8. In this region, the vertical transition of O_3 near the tropopause is characterized by a weaker vertical gradient and broader PDFs relative to that in the tropics (Figure 5). MOZART-3.1 tends to have higher O_3 concentrations in the lower stratosphere than MLS in spring (MAM), which is clearly shown by the difference between the solid and dotted lines in Figure 8. At higher TPRH levels than 3.3 km, MLS and MOZART-3.1 show better agreement except summertime (JJA) according to the low S values. As the bottom plot of Figure 8 displays, in summer (JJA), O_3 in MLS and MOZART-3.1 commonly show weak secondary peaks above the 5 km level around 2–3 ppmv. However, the disagreement of the secondary peak values result in the lower S compared to other seasons.

[31] For H_2O at midlatitudes, MOZART-3.1 did not reproduce low H_2O shown in the MLS observation. This causes the discrepancy and low S values between MLS and MOZART-3.1 in Figure 9. High heel shaped PDFs [*Hegglin et al.*, 2009] in the upper troposphere are one distinguishing characteristic present in both data from the model and observation. The bifurcation of H_2O PDFs during summer and fall is clearly visible below 2.2 km in the TPRH whereas the multiple peaks in O_3 PDFs are shown above 3.3 km in the TPRH.

[32] The existence of multiple peaks in the O_3 and H_2O PDFs indicates that there may be two distinct air masses characterized by different tracer mixing ratios. In addition, the difference in those locations for O_3 and H_2O means that the distinct air masses are transported throughout the UTLS but cause the multimodal distributions where each tracer originally has large variability related to large vertical and latitudinal gradients. The bi-modal structure in PDFs at midlatitudes might be related to the horizontal transport of air columns in the UTLS region since higher O_3 and lower H_2O are shown in lower latitudes than midlatitudes in the TPRH. *Pan et al.* [2004] has shown that changes in the tropopause height can accompany the transport process from lower latitude and *Pan et al.* [2009] interpreted it as the secondary tropopause as a result of tropical air intrusion into the midlatitudes.

[33] *Rood et al.* [2000] has shown that the change in tropopause height is linked to the transport processes of Rossby waves. In this study, we grouped PDFs of tracers according to the tropopause height and examined the transport processes in MOZART-3.1 and MLS. These grouped PDFs are called conditional PDFs. We use a tropopause reference height of 14 km as in *Pan et al.* [2004] to separate air of distinct tropical origin. *Pan et al.* [2009] demonstrated that the tropical air intrusion is related to a low static stability. Figure 10 shows 2-D meridional cross-sections of mean zonal wind, isentropic surfaces, tropopause height and static stability ($d\theta/dz$) in GEOS4 meteorological fields for lower and higher tropopause cases than 14 km at 45°N in September. It is obvious that high tropopause occurrences are related to low static stability between 12 and 15 km. This indicates that

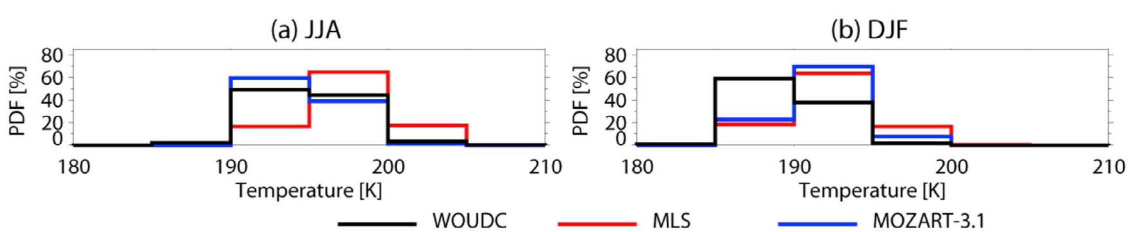

Figure 7. PDFs of cold point temperature near the tropopause level in the tropics (5°S–5°N) for (a) June–August and for (b) December–February. The black, red and blue lines are PDFs from WOUDC, MLS and MOZART-3.1 respectively. WOUDC sonde data is only for tropical Indian Ocean (10°S–10°N and 30°E–120°E).

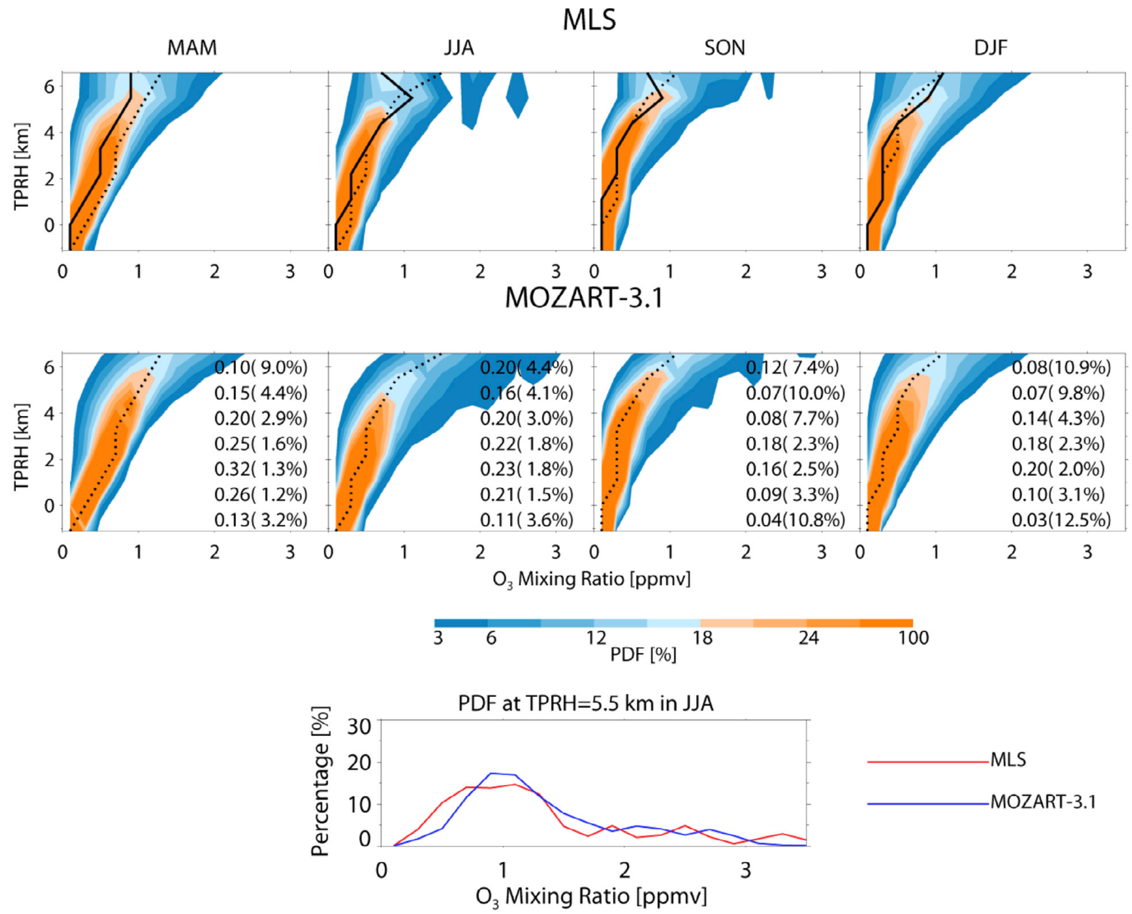

Figure 8. (top and middle) Same as Figure 6 but for O_3 at NH midlatitudes (40°N–50°N). (bottom) PDFs at TPRH level of 5.5 km in JJA from the second column of the PDFs above.

the data classification with a reference tropopause height of 14 km can be a good diagnostic for the tropical air intrusion.

[34] During high tropopause events (>14 km), both MOZART-3.1 and MLS O_3 PDFs in the tropics and midlatitudes look similar while during low tropopause events there are distinct differences (Figure 11) from the high tropopause case. When the tropopause is lower than 14 km, O_3 increases gradually with height while O_3 for the higher tropopause events has a steeper vertical gradient. For quantitative comparison, Table 1 shows the Hellinger distances and S values for the PDFs displayed in Figure 11 with two important messages. When comparing PDFs only for high tropopause cases, S becomes larger at all levels than the S values in the second column of Figure 8. Therefore, when comparing model data with observation in the midlatitudes UTLS, it is important to consider changes of tropopause heights. This is because different frequencies of higher tropopause in the real and model atmosphere can make the difference in the structure of PDFs and large variability shown in PDFs is related to a dynamical process. Also the largest Hellinger distance can be found between the two MLS PDFs for the low and high tropopause cases. As shown in Figure 11, PDFs at midlatitudes for high tropopause cases are similar to those in the tropics showing smaller Hellinger distances above 2.2 km in the TPRH. As discussed previously, the similarity between the tropics and high tropopause case is applicable where tracers show large variability and large gradients vertically and latitudinally. Therefore, for O_3, considering conditional PDFs is needed at higher levels than 2 km in the TPRH.

[35] The vertical gradient of H_2O is greater than O_3 in the UT while O_3 increases more greatly than H_2O in the LS. Accordingly, the lower tropopause at midlatitudes means more abundant H_2O in the upper troposphere below the tropopause. Profiles of H_2O PDFs sorted by tropopause heights in Figure 12 show that the bifurcated H_2O PDFs can be clearly separated. Although the low H_2O is not reproduced, MOZART-3.1 simulations have common patterns with the observations from MLS in the vertical profiles of their PDFs for each high or low tropopause case. PDFs for low and high tropopause cases are clearly distinct as illustrated by their Hellinger distances and S values in Table 2. Differently from O_3, conditional PDFs do not show better agreement between MLS and MOZART-3.1 at the entire levels. However, the highly increased S values demonstrate that it is important to consider the change of tropopause height in H_2O PDF at least at -1.1 and 0 km levels. Again, there are similarities between H_2O and O_3 according to Hellinger distances. However, the similarity for H_2O between separated PDFs for high tropopause cases at midlatitudes and all PDFs in tropics is shown only below 4 km in TPRH where H_2O has large horizontal and vertical gradients.

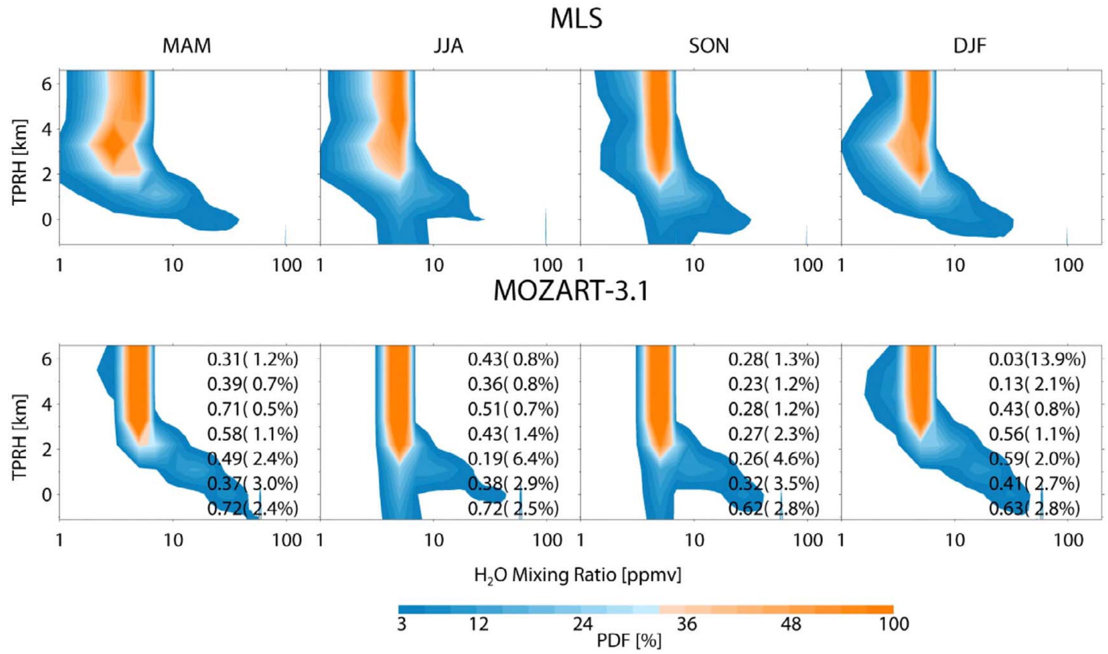

Figure 9. Same as Figure 8 but for H_2O.

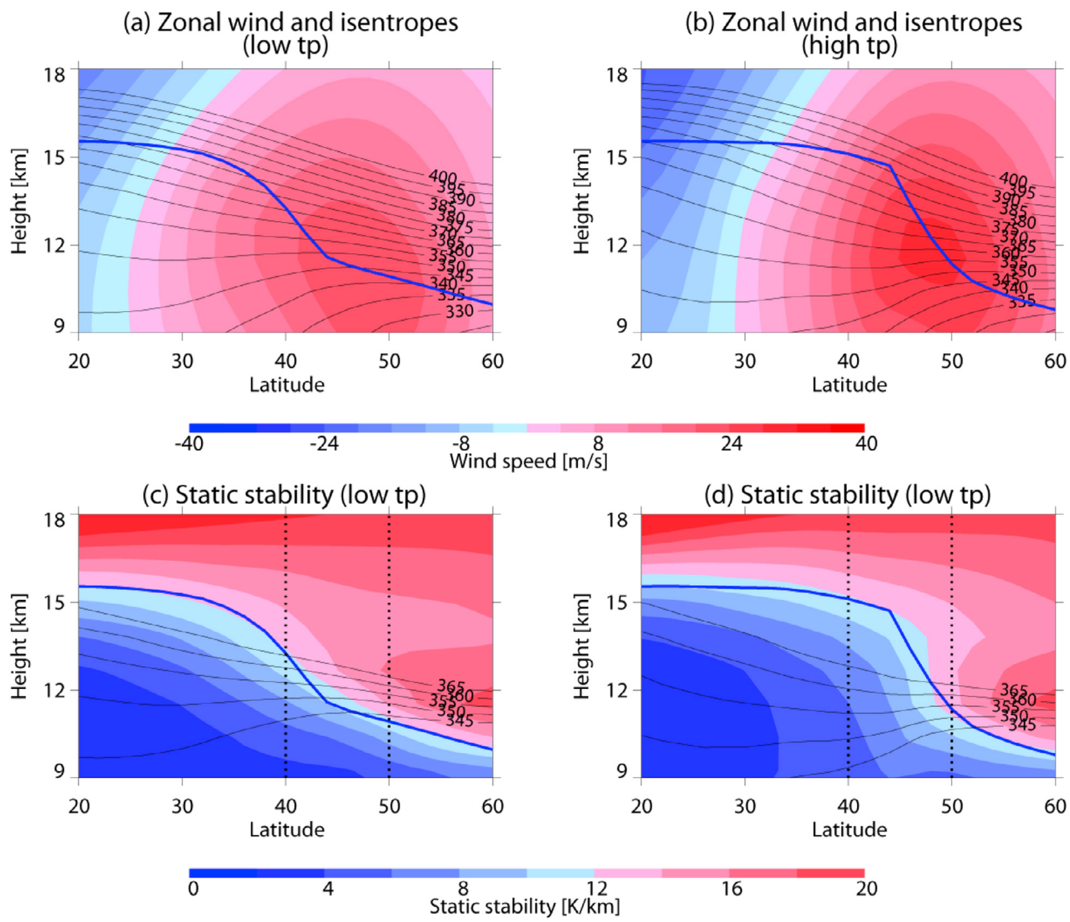

Figure 10. (a and b) Latitude-height cross-sections of mean zonal wind speed, and mean static stability for (c) lower and (d) higher tropopause cases in September. Blue and black solid lines are overplotted to represent mean tropopause heights and isentropes respectively.

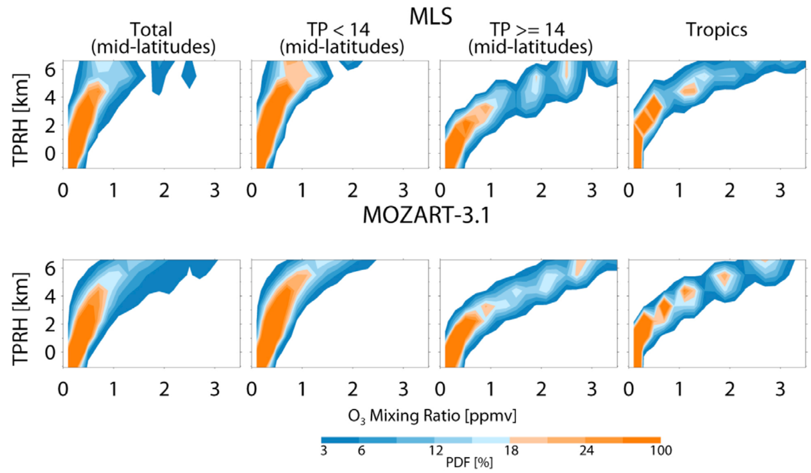

Figure 11. Vertical distribution of O_3 PDFs at NH midlatitudes (40°N–50°N) and in the tropics (5°S–5°N) from (top) MLS and (bottom) MOZART-3.1 in JJA. PDFs at midlatitudes are sorted by tropopause height: from left to right, total PDFs at midlatitudes, PDFs when the tropopause is lower than 14 km, PDFs when the tropopause is higher than 14 km and total PDFs in the tropics.

4.2. Tracer-Tropopause Height Correlation

[36] In the previous section, we analyzed PDFs of tracers in the TPRH and showed the importance of classifying observed and simulated data by tropopause heights to consider the change caused by tropical air intrusion events. We here show how the varying tropopause height and related transport process change tracer distributions in the isobaric coordinate. We made two-dimensional correlation maps between tropopause height (TPH) and O_3 at five isobaric surfaces (46.4, 68.1, 100, 146.8 and 215.4 hPa). Simulated O_3 mixing ratios from MOZART-3.1 on the five isobaric surfaces were estimated by linearly interpolating O_3 from the MOZART-3.1 sigma levels to the pressure levels. We calculated PDFs of O_3 for ten ranges of tropopause heights (5.5∼16.5 km at 1.1 km intervals) and Figure 13 shows the 2-D tropopause height-O_3 PDFs at five isobaric levels. Dashed lines are the most probable values of the PDFs at each tropopause height range. At midlatitudes there are distinguishable changes in vertical profiles of O_3 with varying tropopause height. In both MLS and MOZART-3.1, O_3 mixing ratios are lower throughout the UTLS region for the higher tropopause cases. The decrease in O_3 with increase in tropopause height is largest at 68.1 hPa. This low O_3 at 68.1 hPa corresponds to the air intrusion from the tropics above the level of subtropical jet [*Pan et al.*, 2009]. When the tropopause is higher than 15 km at midlatitudes, O_3 mixing ratios at 68.1 hPa are less than half of the O_3 mixing ratios when the tropopause is lower than 10 km. O_3 mixing ratios in MOZART-3.1 decrease more rapidly as tropopause heights increase than O_3 in MLS data, with a larger decrease of the most probable values (see the dashed lines in Figure 13). Therefore, the high tropopause occurrence at midlatitudes affects O_3 concentrations at several pressure levels in the UTLS.

[37] In general, a higher tropopause correlates well with a decrease in O_3 mixing ratios in both the MOZART-3.1 simulations and MLS observations. To further analyze the changes at midlatitudes, we apply a representative metric to facilitate evaluating the transport from the tropics to midlatitudes to MLS and MOZART-3.1. A metric, g, as defined in *Douglass et al.* [1999] was calculated to evaluate the performance of MOZART-3.1 concisely:

$$g = 1 - \frac{|\mu_{model} - \mu_{observation}|}{n_g \sigma_{observation}} \quad (3)$$

where μ, σ, n are the mean, standard deviation and scale factor, respectively. The g value of near 1 indicates good agreement between the model and observations. Here we used $n_g = 2$ to make all g values positive at the levels considered during the summertime. This also means that overall

Table 1. Hellinger Distance and S Values in Percent Between O_3 PDFs in Figure 11 at Seven TPRH Levels (−1.1 to 5.5 km)

TPRH (km)	Between MLS and MOZART-3.1			Within MLS	
	Total	Low TP	High TP	Low and High TP	High TP and Tropics
5.5	0.196 (3.85%)	0.223 (2.19%)	0.329 (4.15%)	0.969 (0.51%)	0.547 (1.40%)
4.4	0.163 (3.61%)	0.197 (1.95%)	0.251 (4.80%)	0.884 (0.44%)	0.540 (1.14%)
3.3	0.196 (2.36%)	0.250 (1.25%)	0.177 (6.20%)	0.795 (0.39%)	0.649 (0.71%)
2.2	0.220 (1.65%)	0.267 (1.02%)	0.095 (8.98%)	0.511 (0.53%)	0.576 (0.57%)
1.1	0.228 (1.27%)	0.274 (1.16%)	0.097 (6.92%)	0.264 (1.20%)	0.573 (0.45%)
0	0.208 (1.32%)	0.245 (1.01%)	0.076 (8.69%)	0.127 (1.96%)	0.476 (0.45%)
−1.1	0.115 (2.38%)	0.145 (2.52%)	0.052 (10.80%)	0.149 (2.45%)	0.303 (0.81%)

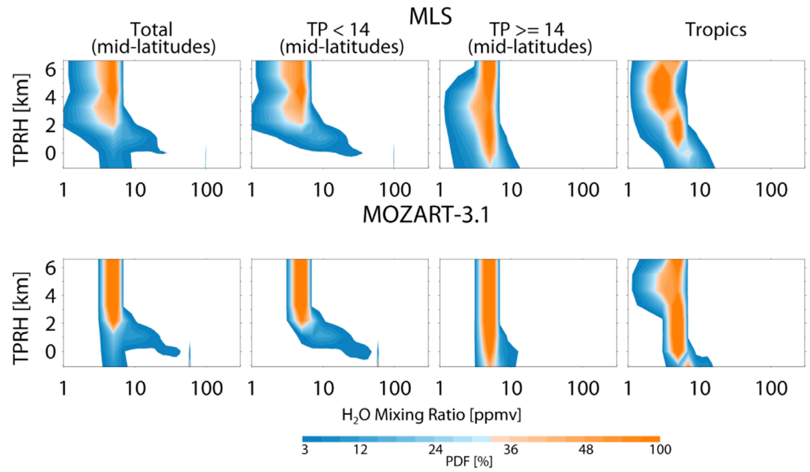

Figure 12. Same as Figure 11 but for H_2O.

the difference between the model and observation is within 2σ range.

[38] In each case, the average and standard deviation of O_3 were calculated. Separated comparison of O_3 between MLS and MOZART-3.1 for low and high tropopause cases allows better model evaluation relative to observed data by minimizing discrepancies due to different frequency of higher tropopause heights between the real atmosphere and the model. Also the difference in mixing ratios between the two groups shows the dependence of tracer concentrations on tropopause heights.

[39] Figure 14 displays g values at five isobaric levels (46.4, 68.1, 100, 146.8 and 215.4 hPa). MOZART-3.1 and MLS show good agreement (noted by large g values and red color) during the low tropopause (<14 km) events at midlatitudes below 46.4 hPa. However, during high tropopause events, there are some discrepancies especially in March. The g values are lower than 0.5 at all levels except 215.4 hPa. This suggests that GEOS4 GCM meteorological fields do not fully represent horizontal transport between the lower latitudes and midlatitudes in spring time.

[40] To further examine the dependence of O_3 on tropopause height, we calculated mean concentrations of O_3 for low and high tropopause cases separately and subtracted the high tropopause mean O_3 from low tropopause O_3. The resulting difference in the mean O_3 for the low and high tropopause cases has an annual variation both in MLS and MOZART-3.1 (Figure 15). The relatively stronger annual variation at 46.4 hPa may be related to stronger activity of planetary waves in winter and spring. MOZART-3.1 O_3 shows similar differences from June through October when there are more frequent high tropopause cases. However, between November and June, the sensitivity of simulated O_3 to the tropopause height is quite different from that of observed O_3 especially at 46.4 and 100 hPa. In MOZART-3.1, the largest O_3 difference occurs in February whereas MLS O_3 is most sensitive to tropopause height changes in March. This disagreement of peak sensitivity is likely the main reason for low g values shown in Figure 14 and lower overall performance of MOZART-3.1 for high tropopause cases in March. Around March, high tropopause events do not occur as frequently as in the summertime. Therefore the overall effect of this erroneous representation of high tropopause in the model can be balanced by much more frequent low tropopause cases so that the total average is similar to observations.

[41] As a potential application of the tropopause sensitivity analyses, Figure 16 shows how the impacts of aviation emissions at midlatitudes in the summertime can differ by changing tropopause heights. The O_3 perturbation is the difference between two MOZART-3.1 simulation results with and without aviation emissions representing the year 1999. The aviation emission data were provided by the Boeing company [*Baughcum et al.*, 1998, also personal communication, 2008] and the total annual NO emission from aircraft is 1.347 Tg. Other than the existence of time-independent aviation emissions, all other conditions were kept the same for the two analyses. The reduction in the O_3 perturbation shown in Figure 16 for the high tropopause cases is significant compared to the total impacts of aviation emissions on the UTLS O_3 (up to several ppbv). This indicates a two-way

Table 2. Same as Table 1 but for H_2O PDFs in Figure 12

	Between MLS and MOZART-3.1			Within MLS	
TPRH (km)	Total	Low TP	High TP	Low and High TP	High TP and Tropics
5.5	0.432 (0.86%)	0.495 (0.89%)	0.198 (1.43%)	0.322 (1.37%)	0.595 (0.42%)
4.4	0.359 (0.88%)	0.345 (1.02%)	0.415 (0.70%)	0.087 (4.01%)	0.468 (0.56%)
3.3	0.510 (0.74%)	0.512 (0.80%)	0.500 (1.30%)	0.178 (2.30%)	0.142 (1.45%)
2.2	0.429 (1.68%)	0.443 (1.80%)	0.413 (1.78%)	0.320 (2.49%)	0.052 (8.37%)
1.1	0.189 (5.64%)	0.205 (5.70%)	0.254 (3.24%)	0.661 (1.77%)	0.081 (5.25%)
0	0.381 (2.60%)	0.419 (2.61%)	0.242 (6.73%)	0.818 (1.34%)	0.274 (3.31%)
−1.1	0.717 (1.61%)	0.810 (1.63%)	0.256 (9.76%)	0.831 (1.59%)	0.283 (4.04%)

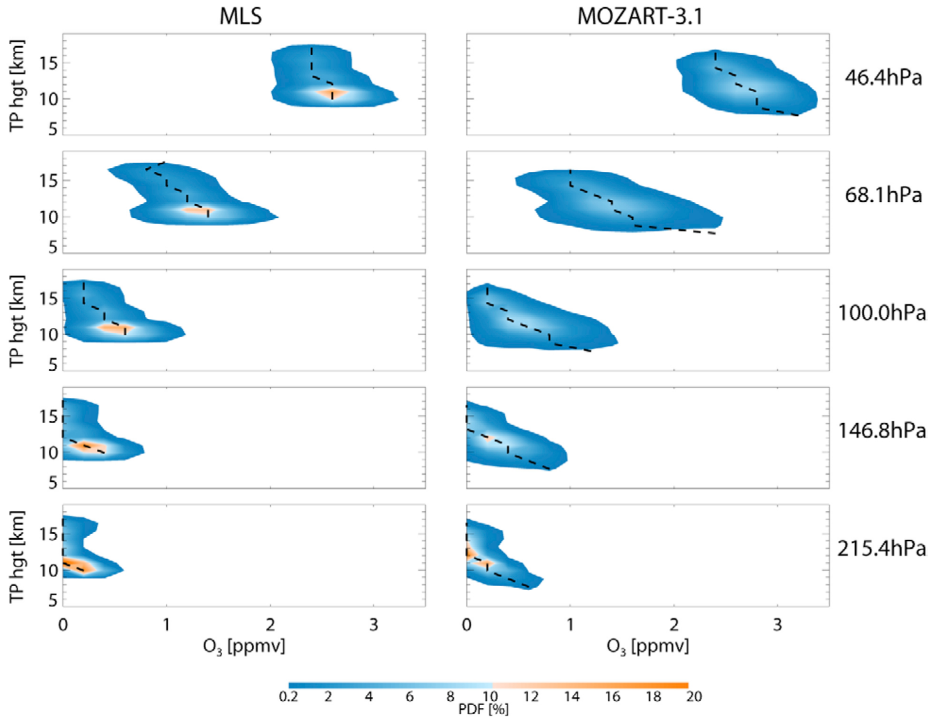

Figure 13. Two dimensional probability density functions at NH midlatitudes (40°N–50°N) during JJA season showing the relationship of O_3 (x axis) and tropopause heights (y axis) for (left) MLS and (right) MOZART 3.1 at five isobaric levels (top to bottom: 46.4, 68.1, 100, 146.8 and 215.4 hPa). Dashed lines connect the most probable values of each tropopause height range.

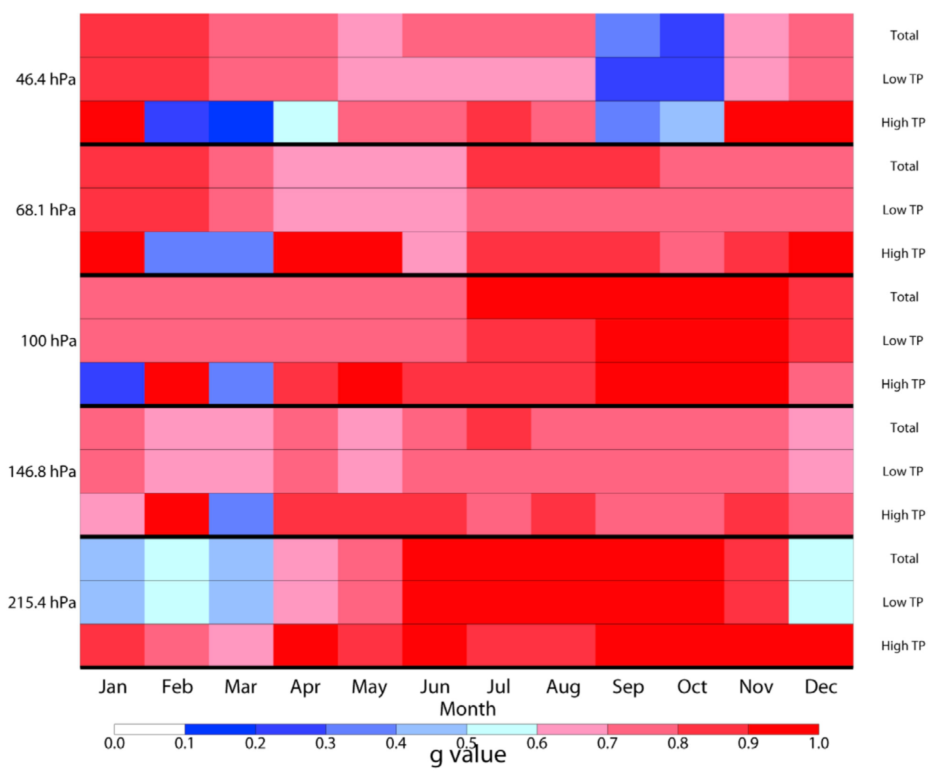

Figure 14. The temporal variation of g values between MOZART-3.1 and MLS on five isobaric surfaces (46.4, 68.1, 100, 146.8 and 215.4 hPa) at midlatitudes (40°N–50°N). At each level, g values for the total data, low tropopause (≤14 km) and high tropopause (>14 km) are shown separately.

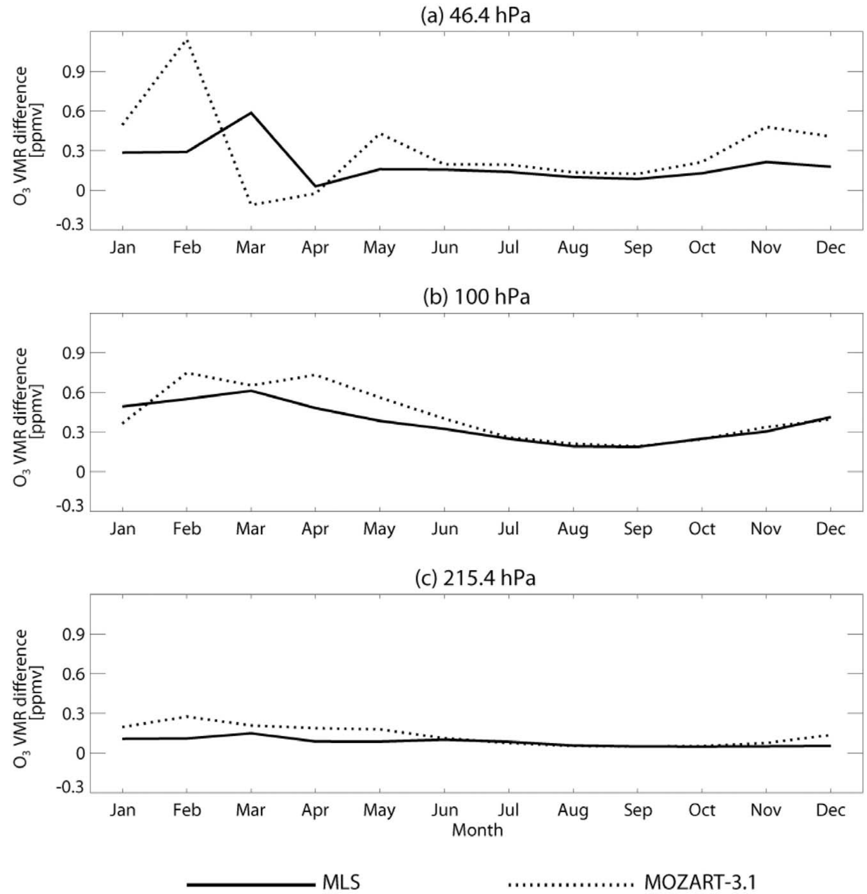

Figure 15. Time series of O_3 differences (O_3 for low tropopause minus O_3 for high tropopause) on (a) 46.4, (b) 100, and (c) 215.4 hPa isobaric surfaces from MLS observation (solid lines) and MOZART-3.1 (dotted lines). The average of O_3 differences is taken at Northern Hemisphere midlatitudes (40°N–50°N) and is calculated each month.

exchange between the tropics and midlatitudes. The tropical air intrusion is related to spreading the impact of aviation emissions that are concentrated in the NH midlatitudes at cruise altitudes (8–10 km) to the lower latitudes where there is less air traffic. Considering the trend of increasing tropopause heights [*Gettelman et al.*, 2011] and expected increase in air traffic and aviation emissions in the future, atmospheric models will need to accurately represent these quasi-horizontal exchange processes and their dependence on tropopause height for the future projection of aviation impacts. Diagnostic tools and analyses such as those

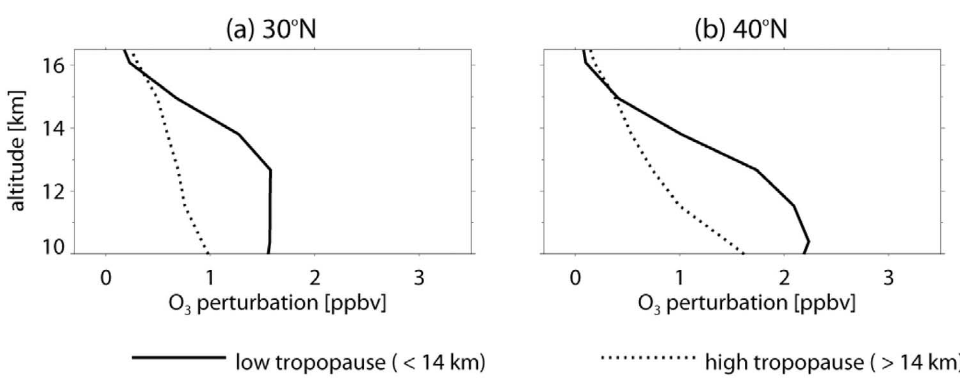

Figure 16. Zonally averaged O_3 perturbation due to the time-independent aviation emissions at (a) 30°N and (b) 40°N latitudes. Solid and dotted lines are the mean perturbations for lower and higher tropopause cases than 14 km respectively.

presented here will be a key in evaluating these model simulated processes relative to observations.

5. Summary and Conclusions

[42] In this study, we utilized several model diagnostics found in previous studies and proposed a comprehensive set of effective methods for diagnosing the tropical air intrusions into the midlatitudes in the UTLS region. A representative CTM simulation using the MOZART-3.1 model driven by a single year GCM meteorological fields for current atmospheric conditions was evaluated using the MLS observational data set with an emphasis on the quasi-horizontal transport in the NH midlatitudes in summer.

[43] We found that the analysis of the data in the TPRH vertical coordinate is more advantageous in revealing detailed vertical structures of tracer profiles in the UTLS region than in conventional altitude coordinates. The adoption of the TPRH vertical coordinate will thus help to increase potential usefulness of satellite data with low vertical resolution in the UTLS.

[44] When the tropopause (TPRH = 0) at midlatitudes is highly varying especially in the NH summer, a large number of vertical tracer profiles in the TPRH coordinate near the UTLS are characterized with multiple peak features in vertical distributions of their PDFs at midlatitudes. The multiple peaks shown in PDFs can be split into separate profiles with each single peak when tracer data are classified or filtered out by the tropopause height. The clear separation of vertical tracer profiles for high tropopause heights from the total data shows impacts of the transported tropical air on the tracer distributions at midlatitudes. The altitude where the tracer is affected by the tropical air intrusion is different for each tracer and depends on the vertical and horizontal gradients of the tracer.

[45] Based on the diagnostics of using the TPRH coordinate and PDF analysis, a MOZART-3.1 simulation driven by GEOS4 meteorological fields is evaluated relative to the MLS data. The difference between observed and modeled PDFs was significant and none of the PDF pairs (observation versus model) satisfied the same population assumption. However, Hellinger distance and newly defined S metric are useful quantitative metrics and applicable to various intercomparison projects handling multiple models and observations. Despite the poor agreement of PDFs between MOZART-3.1 and MLS, the model reproduced the changes of tracer distributions near the tropopause related to the quasi-horizontal STE. In terms of the pattern similarity between vertical tracer PDF distributions in the tropics and for high tropopause midlatitudes cases, MOZART-3.1 agrees well with MLS. When model tracer PDFs in the UTLS are classified by the tropopause height, the difference in dynamical fields between real and GCM atmospheres becomes less significant in comparison. Based on the low static stability and the change in S values, comparing patterns of PDFs between the tropics and high tropopause at midlatitudes is a good tool to evaluate the model's capability for treating intrusions of air from the tropics into the midlatitudes.

[46] Since most model outputs provide tracer concentrations at isobaric levels, correlation maps between tracer concentrations on isobaric surfaces according to tropopause heights are more practical than diagnostics in the TPRH coordinate that require data rearrangement. The dependence of key species on tropopause heights in the UTLS was used to design a useful tool to test the impact of the transport of tropical air parcels on the distributions of chemicals at isobaric levels. The sensitivity of O_3 at isobaric levels to tropopause heights shows the potential to be the basis of a good evaluation tool for chemistry transport and chemistry climate models especially for studying aviation impacts on climate.

[47] Only one model was used in this study and thus it is not known whether MOZART-3.1 shows good performances relative to other CTMs. However, by applying the same tools to various CTMs or CCMs, the resulting differences and identification of related mechanisms could be quantified.

[48] **Acknowledgments.** The authors would like to thank the Federal Aviation Administration (FAA), Aviation Climate Change Research Initiative (ACCRI) for support under contract 10-C-NE-UI amendment 001 and The Partnership for AiR Transportation Noise and Emissions Reduction (PARTNER). Daeok Youn was supported in part by Chungbuk National University. The opinions, findings, and conclusions or recommendations expressed in this material are those of the authors and do not necessarily reflect the views of ACCRI, PARTNER, or the FAA. The satellite data used in this effort were acquired as part of the activities of NASA's Science Mission Directorate, and are archived and distributed by the Goddard Earth Sciences (GES) Data and Information Services Center (DISC).

References

Baughcum, S. L., D. J. Sutkus Jr., and S. C. Henderson (1998), Year 2015 aircraft emission scenario for scheduled air traffic, *NASA-CR-1998–207638*, 44 pp., NASA Langley Res. Cent., Hampton, Va.

Chen, P. (1995), Isentropic cross-tropopause mass exchange in the extratropics, *J. Geophys. Res.*, *100*(D8), 16,661–16,673, doi:10.1029/95JD01264.

Considine, D. B., J. A. Logan, and M. A. Olsen (2008), Evaluation of near-tropopause ozone distributions in the Global Modeling Initiative combined stratosphere/troposphere model with ozonesonde data, *Atmos. Chem. Phys.*, *8*(9), 2365–2385, doi:10.5194/acp-8-2365-2008.

Corder, G. W., and D. I. Foreman (2009), *Nonparametric Statistics for Non-statisticians: A Step-By-Step Approach*, 247 pp., John Wiley, Hoboken, N. J.

Cristofanelli, P., et al. (2003), Stratosphere-to-troposphere transport: A model and method evaluation, *J. Geophys. Res.*, *108*(D12), 8525, doi:10.1029/2002JD002600.

Dessler, A. E., et al. (1995), Correlated observations of HCl and $ClONO_2$ from UARS and implications for stratospheric chlorine partitioning, *Geophys. Res. Lett.*, *22*(13), 1721–1724, doi:10.1029/95GL01593.

Douglass, A. R., M. J. Prather, T. M. Hall, S. E. Strahan, P. J. Rasch, L. C. Sparling, L. Coy, and J. M. Rodriguez (1999), Choosing meteorological input for the global modeling initiative assessment of high-speed aircraft, *J. Geophys. Res.*, *104*(D22), 27,545–27,564, doi:10.1029/1999JD900827.

Emmons, L. K., D. A. Hauglustaine, J. F. Muller, M. A. Carroll, G. P. Brasseur, D. Brunner, J. Staehelin, V. Thouret, and A. Marenco (2000), Data composites of airborne observations of tropospheric ozone and its precursors, *J. Geophys. Res.*, *105*(D16), 20,497–20,538, doi:10.1029/2000JD900232.

Eyring, V., et al. (2010), SPARC report on the evaluation of chemistry-climate models, *SPARC Rep. 5*, Univ. of Toronto, Toronto, Ont., Canada. [Available at http://www.atmosp.physics.utoronto.ca/SPARC.]

Fischer, H., F. G. Wienhold, P. Hoor, O. Bujok, C. Schiller, P. Siegmund, M. Ambaum, H. A. Scheeren, and J. Lelieveld (2000), Tracer correlations in the northern high latitude lowermost stratosphere: Influence of cross-tropopause mass exchange, *Geophys. Res. Lett.*, *27*(1), 97–100, doi:10.1029/1999GL010879.

Forster, P. M. D. F., and K. P. Shine (2002), Assessing the climate impact of trends in stratospheric water vapor, *Geophys. Res. Lett.*, *29*(6), 1086, doi:10.1029/2001GL013909.

Forster, P. M. D. F., and K. Tourpali (2001), Effect of tropopause height changes on the calculation of ozone trends and their radiative forcing, *J. Geophys. Res.*, *106*(D11), 12,241–12,251, doi:10.1029/2000JD900813.

Gettelman, A., D. E. Kinnison, T. J. Dunkerton, and G. P. Brasseur (2004), Impact of monsoon circulations on the upper troposphere and lower stratosphere, *J. Geophys. Res.*, *109*, D22101, doi:10.1029/2004JD004878.

Gettelman, A., et al. (2010), Multimodel assessment of the upper troposphere and lower stratosphere: Tropics and global trends, *J. Geophys. Res.*, *115*, D00M08, doi:10.1029/2009JD013638.

Gettelman, A., P. Hoor, L. L. Pan, W. J. Randel, M. I. Hegglin, and T. Birner (2011), The extratropical upper troposphere and lower stratosphere, *Rev. Geophys.*, *49*, RG3003, doi:10.1029/2011RG000355.

Hegglin, M. I., and T. G. Shepherd (2007), O_3-N_2O correlations from the Atmospheric Chemistry Experiment: Revisiting a diagnostic of transport and chemistry in the stratosphere, *J. Geophys. Res.*, *112*, D19301, doi:10.1029/2006JD008281.

Hegglin, M. I., C. D. Boone, G. L. Manney, T. G. Shepherd, K. A. Walker, P. F. Bernath, W. H. Daffer, P. Hoor, and C. Schiller (2008), Validation of ACE-FTS satellite data in the upper troposphere/lower stratosphere (UTLS) using non-coincident measurements, *Atmos. Chem. Phys.*, *8*(6), 1483–1499, doi:10.5194/acp-8-1483-2008.

Hegglin, M. I., C. D. Boone, G. L. Manney, and K. A. Walker (2009), A global view of the extratropical tropopause transition layer from Atmospheric Chemistry Experiment Fourier Transform Spectrometer O_3, H_2O, and CO, *J. Geophys. Res.*, *114*, D00B11, doi:10.1029/2008JD009984.

Hegglin, M. I., et al. (2010), Multimodel assessment of the upper troposphere and lower stratosphere: Extratropics, *J. Geophys. Res.*, *115*, D00M09, doi:10.1029/2010JD013884.

Holton, J. R., P. H. Haynes, M. E. Mcintyre, A. R. Douglass, R. B. Rood, and L. Pfister (1995), Stratosphere-troposphere exchange, *Rev. Geophys.*, *33*(4), 403–439, doi:10.1029/95RG02097.

Hoor, P., H. Fischer, L. Lange, J. Lelieveld, and D. Brunner (2002), Seasonal variations of a mixing layer in the lowermost stratosphere as identified by the CO-O_3 correlation from in situ measurements, *J. Geophys. Res.*, *107*(D5), 4044, doi:10.1029/2000JD000289.

Hoor, P., C. Gurk, D. Brunner, M. I. Hegglin, H. Wernli, and H. Fischer (2004), Seasonality and extent of extratropical TST derived from in-situ CO measurements during SPURT, *Atmos. Chem. Phys.*, *4*, 1427–1442, doi:10.5194/acp-4-1427-2004.

Kim, J., and S.-W. Son (2012), Tropical cold-point tropopause: Climatology, seasonal cycle and intraseasonal variability derived from COSMIC GPS radio occultation measurements, *J. Clim.*, *25*, 5343–5360, doi:10.1175/JCLI-D-11-00554.1.

Kinnison, D. E., et al. (2007), Sensitivity of chemical tracers to meteorological parameters in the MOZART-3 chemical transport model, *J. Geophys. Res.*, *112*, D20302, doi:10.1029/2006JD007879.

Lacis, A. A., D. J. Wuebbles, and J. A. Logan (1990), Radiative forcing of climate by changes in the vertical distribution of ozone, *J. Geophys. Res.*, *95*(D7), 9971–9981, doi:10.1029/JD095iD07p09971.

Li, Q. B., et al. (2005), Convective outflow of South Asian pollution: A global CTM simulation compared with EOS MLS observations, *Geophys. Res. Lett.*, *32*, L14826, doi:10.1029/2005GL022762.

Liu, C. X., Y. Liu, H. P. Wang, X. X. Tie, S. T. Gao, D. Kinnison, and G. Brasseur (2009), Atmospheric tracers during the 2003–2004 stratospheric warming event and impact of ozone intrusions in the troposphere, *Atmos. Chem. Phys.*, *9*(6), 2157–2170, doi:10.5194/acp-9-2157-2009.

Livesey, N. J., et al. (2011), MLS Version 3.3 Level 2 data quality and description document, *Tech. Rep. JPL D-33509*, Jet Propul. Lab., Pasadena, Calif. [Available at http://mls.jpl.nasa.gov.]

Manney, G. L., et al. (2007), Solar occultation satellite data and derived meteorological products: Sampling issues and comparisons with Aura Microwave Limb Sounder, *J. Geophys. Res.*, *112*, D24S50, doi:10.1029/2007JD008709.

Manney, G. L., et al. (2011), Jet characterization in the upper troposphere/lower stratosphere (UTLS): Applications to climatology and transport studies, *Atmos. Chem. Phys.*, *11*(12), 6115–6137, doi:10.5194/acp-11-6115-2011.

Mote, P. W., K. H. Rosenlof, J. R. Holton, R. S. Harwood, and J. W. Waters (1995), Seasonal variations of water vapor in the tropical lower stratosphere, *Geophys. Res. Lett.*, *22*(9), 1093–1096, doi:10.1029/95GL01234.

Pan, L. L., W. J. Randel, B. L. Gary, M. J. Mahoney, and E. J. Hintsa (2004), Definitions and sharpness of the extratropical tropopause: A trace gas perspective, *J. Geophys. Res.*, *109*, D23103, doi:10.1029/2004JD004982.

Pan, L. L., J. C. Wei, D. E. Kinnison, R. R. Garcia, D. J. Wuebbles, and G. P. Brasseur (2007), A set of diagnostics for evaluating chemistry-climate models in the extratropical tropopause region, *J. Geophys. Res.*, *112*, D09316, doi:10.1029/2006JD007792.

Pan, L. L., W. J. Randel, J. C. Gille, W. D. Hall, B. Nardi, S. Massie, V. Yudin, R. Khosravi, P. Konopka, and D. Tarasick (2009), Tropospheric intrusions associated with the secondary tropopause, *J. Geophys. Res.*, *114*, D10302, doi:10.1029/2008JD011374.

Ray, E. A., K. H. Rosenlof, E. Richard, D. Parrish, and R. Jakoubek (2004), Distributions of ozone in the region of the subtropical jet: An analysis of in situ aircraft measurements, *J. Geophys. Res.*, *109*, D08106, doi:10.1029/2003JD004143.

Reichler, T., M. Dameris, and R. Sausen (2003), Determining the tropopause height from gridded data, *Geophys. Res. Lett.*, *30*(20), 2042, doi:10.1029/2003GL018240.

Rieder, H. (2005), *Robust Asymptotic Statistics*, 2nd ed., Springer, New York.

Rood, R. B., A. R. Douglass, M. C. Cerniglia, L. C. Sparling, and J. E. Nielsen (2000), Seasonal variability of middle-latitude ozone in the lowermost stratosphere derived from probability distribution functions, *J. Geophys. Res.*, *105*(D14), 17,793–17,805, doi:10.1029/2000JD900142.

Rosenlof, K. H., A. F. Tuck, K. K. Kelly, J. M. Russell, and M. P. McCormick (1997), Hemispheric asymmetries in water vapor and inferences about transport in the lower stratosphere, *J. Geophys. Res.*, *102*(D11), 13,213–13,234, doi:10.1029/97JD00873.

Sankey, D., and T. G. Shepherd (2003), Correlations of long-lived chemical species in a middle atmosphere general circulation model, *J. Geophys. Res.*, *108*(D16), 4494, doi:10.1029/2002JD002799.

Santee, M. L., G. L. Manney, N. J. Livesey, L. Froidevaux, M. J. Schwartz, and W. G. Read (2011), Trace gas evolution in the lowermost stratosphere from Aura Microwave Limb Sounder measurements, *J. Geophys. Res.*, *116*, D18306, doi:10.1029/2011JD015590.

Solomon, S., K. H. Rosenlof, R. W. Portmann, J. S. Daniel, S. M. Davis, F. J. Sanford, and G.-K. Plattner (2010), Contributions of stratospheric water vapor to decadal changes in the rate of global warming, *Science*, *327*(5970), 1219–1223, doi:10.1126/science.1182488.

Son, S. W., L. M. Polvani, D. W. Waugh, T. Birner, H. Akiyoshi, R. R. Garcia, A. Gettelman, D. A. Plummer, and E. Rozanov (2009), The impact of stratospheric ozone recovery on tropopause height trends, *J. Clim.*, *22*(2), 429–445, doi:10.1175/2008JCLI2215.1.

Sparling, L. C. (2000), Statistical perspectives on stratospheric transport, *Rev. Geophys.*, *38*(3), 417–436, doi:10.1029/1999RG000070.

Strahan, S. E., and B. C. Polansky (2006), Meteorological implementation issues in chemistry and transport models, *Atmos. Chem. Phys.*, *6*, 2895–2910, doi:10.5194/acp-6-2895-2006.

Strahan, S. E., B. N. Duncan, and P. Hoor (2007), Observationally derived transport diagnostics for the lowermost stratosphere and their application to the GMI chemistry and transport model, *Atmos. Chem. Phys.*, *7*(9), 2435–2445, doi:10.5194/acp-7-2435-2007.

Tilmes, S., et al. (2010), An aircraft-based upper troposphere lower stratosphere O_3, CO, and H_2O climatology for the Northern Hemisphere, *J. Geophys. Res.*, *115*, D14303, doi:10.1029/2009JD012731.

Tilmes, S., et al. (2011), Ozonesonde climatology between 1995 and 2009: Description, evaluation and applications, *Atmos. Chem. Phys. Discuss.*, *11*, 28,747–28,796, doi:10.5194/acpd-11-28747-2011.

Waters, J. W., et al. (2006), The Earth Observing System Microwave Limb Sounder (EOS MLS) on the Aura satellite, *IEEE Trans. Geosci. Remote Sens.*, *44*(5), 1075–1092, doi:10.1109/TGRS.2006.873771.

World Meteorological Organization (WMO) (1957), Meteorology: A three-dimensional science, *WMO Bull.*, *4*, pp. 134–138.

Wuebbles, D. J., and K. O. Patten (2009), Three-dimensional modeling of HCFC-123 in the atmosphere: Assessing its potential environmental impacts and rationale for continued use, *Environ. Sci. Technol.*, *43*(9), 3208–3213, doi:10.1021/es802308m.

Youn, D., D. J. Wuebbles, K. O. Patten, and J. T. Lin (2009), Explicit calculation of indirect global warming potentials for halons using atmospheric models, *Atmos. Chem. Phys.*, *9*(22), 8719–8733, doi:10.5194/acp-9-8719-2009.

Youn, D., D. J. Wuebbles, K. O. Patten, H. Lee, and C. W. So (2010), Potential impact of iodinated replacement compounds CF_3I and CH_3I on atmospheric ozone: A three-dimensional modeling study, *Atmos. Chem. Phys.*, *10*(20), 10,129–10,144, doi:10.5194/acp-10-10129-2010.

Zahn, A., and C. A. M. Brenninkmeijer (2003), New directions: A chemical tropopause defined, *Atmos. Environ.*, *37*(3), 439–440, doi:10.1016/S1352-2310(02)00901-9.

Zahn, A., et al. (2000), Identification of extratropical two-way troposphere-stratosphere mixing based on CARIBIC measurements of O_3, CO, and ultrafine particles, *J. Geophys. Res.*, *105*(D1), 1527–1535, doi:10.1029/1999JD900759.

Ziemke, J. R., S. Chandra, B. N. Duncan, L. Froidevaux, P. K. Bhartia, P. F. Levelt, and J. W. Waters (2006), Tropospheric ozone determined from aura OMI and MLS: Evaluation of measurements and comparison with the Global Modeling Initiative's Chemical Transport Model, *J. Geophys. Res.*, *111*, D19303, doi:10.1029/2006JD007089.